



Evolution of coal permeability during gas/energy storage

Chuanzhong Jiang^a, Jishan Liu^{a,*}, Yee-Kwong Leong^a, Derek Elsworth^b

^a School of Engineering, The University of Western Australia, 35 Stirling Highway, Perth, WA, 6009, Australia

^b Department of Energy and Mineral Engineering, G3 Center and Energy Institute, The Pennsylvania State University, University Park, PA, 16802, USA

ARTICLE INFO

Handling Editor: Dr M Mahdi Najafpour

Keywords:

Hydrogen storage
Carbon dioxide sequestration
Coal permeability
Fictitious stress
Effective stress principle

ABSTRACT

Both carbon dioxide and hydrogen can be stored in coal seams as two enabling components of energy transition from fossil-based systems to renewable sources. In both cases, understanding the evolution of coal permeability under the influence of gas adsorption is extremely important. The gas sorption-induced deformation is commonly treated by analogous calculation of thermal expansion. This assumption has long been proved to be inconsistent with observations as reported in the literature. In this study, we hypothesize that the difference between the assumption and the reality is due to self-constrained/facilitated swelling phenomena during gas injection. Under this new hypothesis, coal could be constrained or facilitated depending on coal internal structures and processes. A concept of fictitious stress is introduced to quantify coal self-constrained or facilitated degree and converted into the equivalent effective stress. This conversion has transformed the conventional effective stress principle to unconventional one. This has led to new generic coal permeability model, which has been validated by experimental data. An analysis of stress state evolution during gas storage process is conducted. Our results suggest that our coal permeability model is a valuable tool for evaluation of gas storage in coal seams.

1. Introduction

Carbon neutrality, defined as a state of net-zero carbon emissions, can be realized by equalizing the overall carbon dioxide or greenhouse gas emissions through initiatives that focus on carbon offsetting or removal [1,2]. Achieving carbon neutrality aligns with the Paris Agreement's call of limiting the global temperature rise to within 1.5 °C compared to pre-industrial levels [3]. Among the fundamental strategies for achieving carbon neutrality are the development and utilization of clean energy sources, as well as the application of carbon capture and storage technologies [4]. In this context, hydrogen, as an energy carrier to replace natural gas [5,6], is considered the future of clean energy sources due to its high energy density and relatively low carbon footprint [7,8]. Electricity derived from renewable energy sources, such as geothermal, biomass, hydro, solar and wind, can be employed in the electrolysis of water to produce hydrogen gas [9]. The hydrogen produced can be stored for utilization across various sectors including transportation, industrial, residential, utility, chemical, and agricultural domains [10]. However, due to hydrogen's low volume density, large storage spaces are needed for an industrial-scale hydrogen economy, which surface facilities like tanks and pipelines cannot provide [11]. Additionally, the progressively increasing emissions of greenhouse gases

necessitate the establishment of geological storage sites on a gigatonne scale for sequestration [12]. Consequently, to satisfy the growing demand for carbon neutrality and support the transition to clean energy, there is a need to expand the capacity of repositories for geological storage of both CO₂ and H₂.

Among the various options for underground gas/energy storage sites, coal seams emerge as the optimal choice [13,14]. The primary advantages of coal seams encompass the following aspects: 1. due to its relatively larger surface area, it can adsorb large amounts of CO₂ [15] and H₂ [16–19]; 2. unlike free gas in conventional reservoirs, the chance of leakage for adsorbed gas is minimal [13]; 3. availability of existing surface and subsurface infrastructure for gas injection/production [20]; 4. several prospective locations have been experimented with for storing gases, including CO₂ and flue gas [17]; 5. widely distributed coal seams across the globe have the potential to offer storage capacities at the gigatonne scale [21].

Permeability is one of the important reservoir parameters for the geological storage of CO₂ or hydrogen in coal seams, as it can directly affects the gas injection process [22,23]. The storage mechanism of gases in coal seams primarily relies on the adsorption characteristics of coal [19]. The sorption mechanism in coal seams is believed to be a complex physicochemical process including interactions between the

* Corresponding author.

E-mail address: jishan.liu@uwa.edu.au (J. Liu).

<https://doi.org/10.1016/j.ijhydene.2023.12.133>

Received 26 October 2023; Received in revised form 4 December 2023; Accepted 13 December 2023

0360-3199/© 2023 The Authors. Published by Elsevier Ltd on behalf of Hydrogen Energy Publications LLC. This is an open access article under the CC BY license (<http://creativecommons.org/licenses/by/4.0/>).

gas and the coal matrix [19,24]. Generally, the permeability of coal seams is subject to change due to various influencing factors during the process of gas injection and extraction [25–27]. Wherein, gas adsorption can lead to significant changes in the permeability of coal seams [23, 28]. However, accurately predicting these changes during gas injection remains a challenge. Traditionally, the theory of Poroeasticity suggests that rock mass permeability is governed solely by effective stress [29]. According to this theory, when the effective stress remains constant, permeability should be a constant as predicted by this theory and will not change with the gas type or the injection pressure [30]. This prediction, however, contradicts experimental data [31]. To explain these discrepancies, many permeability models have been derived. Although it is generally believed that the evolution of coal permeability is jointly controlled by the change of effective stress and adsorption [32], experimental data showed that methane desorption would lead to the decrease of effective stress with the decrease of gas pressure [33]. It was also reported that the effective stress acting on coal can be changed by gas adsorption under the triaxial stress condition [34]. How, therefore, to characterize the stresses generated in the process of gas adsorption which are not explicitly included in the effective stress theory becomes the key of resolving this dilemma.

The concept of adsorption stress or the internal stress induced by gas adsorption had been used to represent the effect of gas adsorption [35]. By making an analogy between thermal expansion and matrix swelling associated with gas adsorption in coalbeds [26], the adsorption stress is calculated by measuring the volume expansion and Hooke's law [36]. Despite the fact that this approach has been applied by many works to account for the adsorption stress [37], there are four primary concerns that require our focused attention: 1, the adsorption stress calculated by this method can only reflect the stress under constant volume boundary condition [23]; 2, in this method, coal is assumed to be homogeneous, there will be no thermal stress after the homogeneous expansion deformation reaches equilibrium according to the thermodynamic theory [38], so this method cannot explain the evolution of coal permeability under the condition of free expansion [39]; 3, the differential/heterogeneous swelling strain/stress due to coal heterogeneity/inhomogeneity is missed [40,41]; 4, such treatment do not necessarily follow thermodynamic laws as discussed [42].

The major objective of this study is to characterize the influence of adsorption on effective stress and, based on this, to analyze the evolutionary behavior of coal seam permeability during the process of gas storage. We introduced the self-constrained/facilitated adsorption-swelling concept to describe the heterogeneous swelling process due to the non-uniformly distributed spatial structures. As a measure of self-constrained/facilitated adsorption-swelling behavior, fictitious stress is introduced and incorporated into the conventional effective stress principle. This incorporation has led to a new generic coal permeability model. The model is degenerated into a spectrum of specific models from stress controlled to displacement controlled and are validated through matching observations.

2. Literature review

In unconventional gas reservoirs such as coalbeds and shale reservoirs, the effective stress law is widely used as both gas sorption and effective stress significantly impact the deformability and fracture permeability of these reservoirs. Terzaghi first proposed the effective stress law, in mathematical form, Terzaghi effective stress σ_e^T is expressed as the difference between total stress σ_c and pore-fluid pressure p [43]

$$\sigma_e^T = \sigma_c - p \quad (1)$$

It should be noted that compressive stress is regarded as positive in this context. Terzaghi's treatment represents a specific case of saturated soils with incompressible grains, thereby offering a limited scope of

applicability [44]. Subsequent to Terzaghi's approach, a modified version was introduced for porous media by Biot [45], who proposed the following effective stress law:

$$\sigma_{eij}^B = \sigma_{cij} - \alpha p \delta_{ij} \quad (2)$$

Where σ_e^B is the Biot effective stress tensor, σ_{cij} is the total stress tensor, δ_{ij} is the Kronecker delta, and α is the effective stress constant, which is also known as the Biot coefficient.

The changes in porosity and permeability are believed to be directly related to changes in effective stress [46]. Whereas the relationship between coal permeability change and effective stress change can be defined as [28,29,47].

$$\frac{k}{k_0} = \exp(-3c_f \Delta\sigma_e) \quad (3)$$

Where k_0 is the initial permeability, k denotes the permeability value disturbed by effective stress variation $\Delta\sigma_e$, c_f is the coal fracture compressibility. Coal permeability data can be well explained by Eq. (3) when the flooding gas is non adsorptive gas: when the effective stress decreases, the permeability increases exponentially [47]; when the effective stress keeps constant, the permeability ratio remains unchanged around 1 [48]. However, when this theory is used to explain the experimental data of the permeability as the percolation gas is adsorptive like methane or CO₂, there will be obvious deviation [31]. The reason is that the stress generated in the adsorption process plays a significant role, but has not been incorporated into the effective stress principle [28,39]. Different methods have been tried to incorporate the adsorption/swelling stress into the conventional effective stress principle (normally Eq. (1) and Eq. (2)). 3 types of handling approach about the adsorption/swelling stress can be listed according to specific definitions:

2.1. Type 1. analogous method of calculating thermal expansion stress

For most of the previous works, when it refers to evaluate the effect of adsorption on the change of stress state for unconventional reservoirs, the analogy calculation of thermal expansion stress is usually used [26, 36,37,49].

$$\Delta\sigma_s = K \Delta e_s^V \quad (4)$$

Where $\Delta\sigma_s$ denotes the stress increment induced by gas adsorption, K is the bulk modulus and Δe_s^V is the volumetric strain increment caused by gas adsorption. By incorporating this adsorption stress into the conventional effective stress principle, the increment of effective stress can be rewritten as [23,35,42]

$$\Delta\sigma_e = \Delta\sigma_c - \alpha \Delta p + K \Delta e_s^V \quad (5)$$

According to the theory of thermodynamics, the thermal stress refers to the stress generated as temperature change induced volumetric deformation is completely constrained [38]. Therefore, the adsorption stress calculated by the method of analogy (Eq. (4)) can only reflect the stress state when the adsorption induced volumetric deformation of coal is completely constrained (i.e. constant volume (CV) condition) [42], and Eq. (5) should only represent the effective stress change under the CV boundary. On the other hand, coal is assumed to be a homogeneous material with inherent properties uniformly distributed within a controlled volume, adsorption stress disappeared in the case of unconstrained swelling (also called as free swelling condition), where Eq. (5) degenerated into Eq. (1). However, such assumption is not consistent with experimental data, in which the injection of adsorbed gas will lead to significant changes in coal permeability even under the constant effective stress condition [50].

2.2. Type 2. method of separating adsorption stress

After realizing that utilizing the entire volume swelling deformation caused by adsorption to calculate the adsorption stress may result in an overestimation [51], a secondary approach was proposed, which assumes that only a portion of the volume strain due to adsorption is relevant to the swelling stress [28]. Compared with Eq. (5), a partition coefficient was proposed to calculate the swelling stress:

$$\Delta\sigma_e = \Delta\sigma_c - \alpha\Delta p + f * K\Delta\varepsilon_s^V \quad (6)$$

Where f is a constant between 0 and 1, when f equals to 0, it indicates that adsorption will not lead to the generation of adsorption stress. When f equals to 1, it indicates that all deformation caused by adsorption contributes to the adsorption stress, and this form degenerates into the first type. This approach can better match experimental data to some extent compared to converting all adsorption strains into adsorption stresses, but the physical meaning behind this ratio still needs to be studied.

Type 3. Method of modifying the Biot coefficient.

The Biot's coefficient has traditionally been regarded as a constant. However, in some studies, the Biot coefficient is expressed as a function of the adsorption stress caused by pressure changes, along with the change in effective stress caused by pressure changes, the effective stress law has been extended to sorbing media [44,45]:

$$\Delta\sigma_e = \Delta\sigma_c - \alpha(\varepsilon_s)\Delta p \quad (7)$$

$$\alpha(\varepsilon_s) = 1 - \frac{K}{K_s} + \frac{K\varepsilon_L}{P_L + p} \quad (8)$$

Where $\alpha(\varepsilon_s)$ is the modified Biot coefficient, which is a function of pore pressure and related to coal adsorption parameters, elastic modulus. Although there are different expressions of the Biot coefficient function, the volumetric strain caused by adsorption is still used to calculate the adsorption stress when dealing with the relationship between adsorption strain and adsorption stress. This method, in essence, is only applicable when all the volume deformation caused by adsorption is constrained, that is, the constant volume boundary conditions.

The common feature of the three common treatment methods for adsorption stress summarized above is to limit the expansion deformation of coal (whether it is fully or partially limited) and convert the limited adsorption strain into adsorption stress. This method obviously cannot explain the evolution law of coal permeability without displacement constraint, especially the permeability change behavior under free expansion [31]. Understanding the changes in stress state caused by adsorption under unconstrained boundary conditions is of great significance for interpreting these data.

3. Concept of fictitious stress

In this current effort, the concept of fictitious stress is introduced as an attempt to understand the microscopic basis of adsorption stress and the self-constrained/facilitated adsorption-swelling behavior in coal.

3.1. Self-constrained/facilitated adsorption-swelling behavior

Over the past decades, micro scale characterization of coal structures and gas adsorption caused coal deformation have been captured through the advanced X-ray CT (computerized tomography) and SEM (scanning electron microscopy) [52]. The micro-CT scan results indicated that, by nature, coal is a heterogeneous/inhomogeneous material with different mineral/matrix compositions [53] and heterogeneous pore structures [54,55] randomly distributed inside. The heterogeneous nature of the spatially non-uniform distribution of the coal matrix results in mutual interactions between the internal matrices and fractures during the adsorption swelling process [56,57].

In various studies, this behavior has been observed through X-ray CT or SEM imaging of different coal samples during gas adsorption processes. We have compiled several pieces of evidence from published works and presented them in Fig. 1. The non-uniform change of normalized bulk densities due to CO₂ adsorption show the swelling deformation of matrix are locked by surrounding components [56], as shown in Fig. 1(a). As the most direct response, such heterogeneous swelling and deformation of the matrix will squeeze each other [58], lead to compression of the fracture aperture even in the absence of displacement or loading constraints [52], as shown in Fig. 1 (b). In this paper, we define this phenomenon as a self-constrained adsorption-swelling behavior. Apparently, this self-constrained adsorption-swelling process can be reflected in that the swelling deformation of the matrix is constrained in the microcosm, and a smaller volumetric deformation is measured in the macroscopic [59], as represented in Fig. 1 (c). Where a smaller volumetric strain of coal mass is measured compared to the coal matrix inside. However, there is also evidence that gas adsorption does not always result in mutual binding of internal components. For example, Scanning electron microscopy images show that CO₂ adsorption can also lead to an increase in the opening of coal internal pores [15]. Based on the provided data, the coal samples exhibited a range of microscopic pore opening changes from a 9.1 % decrease to a 17.3 % increase after exposure to CO₂, with an average increase of 10.5 %, as illustrated in Fig. 1 (d). It is obvious that in this special case, adsorption will lead to the enlargement of internal pore aperture and thus facilitate permeability. In this research, we refer to this behavior as the phenomenon of self-facilitated adsorption-swelling. The self-constrained/facilitated adsorption-swelling phenomena is a manifestation of coal heterogeneity during gas adsorption, such behavior leads to internal swelling even in the absence of external confining pressure. Thus, affecting the fracture aperture change and leading to an enigmatic behavior of coal permeability evolution even in the completely free swelling condition. Quantifying the internal swelling strain/stress caused by self-constrained/facilitated adsorption-swelling phenomena will help to analyze the influence of adsorption on the change of reservoir properties.

3.2. Fictitious stress and the unconventional effective stress

In the previous section, we introduced the concept of self-constrained or self-facilitated adsorption-induced swelling behavior in coal. This behavior arises as a macroscopic manifestation due to the mutual constraints or promotions among the microstructural components of the coal. We assume that this macroscopic effect can be represented by a fictitious stress. By employing such homogenization method, the internal stress induced by adsorption in coal can be characterized and eventually incorporated into the conventional effective stress principle.

To start, the four balls represent the Representative Elementary Volume (REV) of coal mass, as shown in Fig. 2 (a). The balls represent the matrix grains, and the voids between the particles represent the pores of coal. The volume of coal mass V_c is composed of the volume of solid matrix grain V_s and pore volume V_p , which is $V_c = V_s + V_p$. Then, by definition, the initial porosity of coal mass can be expressed as $\varphi_0 = V_p/V_c$.

Gas adsorption leads to the swelling of coal matrix [60]. If a homogeneous and isotropic coal is considered, the coal sample will expand completely freely. A uniform swelling caused by gas adsorption will occur at the equilibrium state with a pressure rises by Δp , as shown in Fig. 2 (b). Under this condition, gas adsorption results in proportional expansion of matrix, pores, and coal mass. Thus, the change of matrix strain ($\Delta\varepsilon_m^e$) and coal mass strain ($\Delta\varepsilon_c^e$) is equivalent to the due to the volume change with proportional variation [23]. If we define the coal mass swelling at that condition as the unconstrained swelling case and denote the swelling strain by ε_{s1} , which is the unconstrained swelling

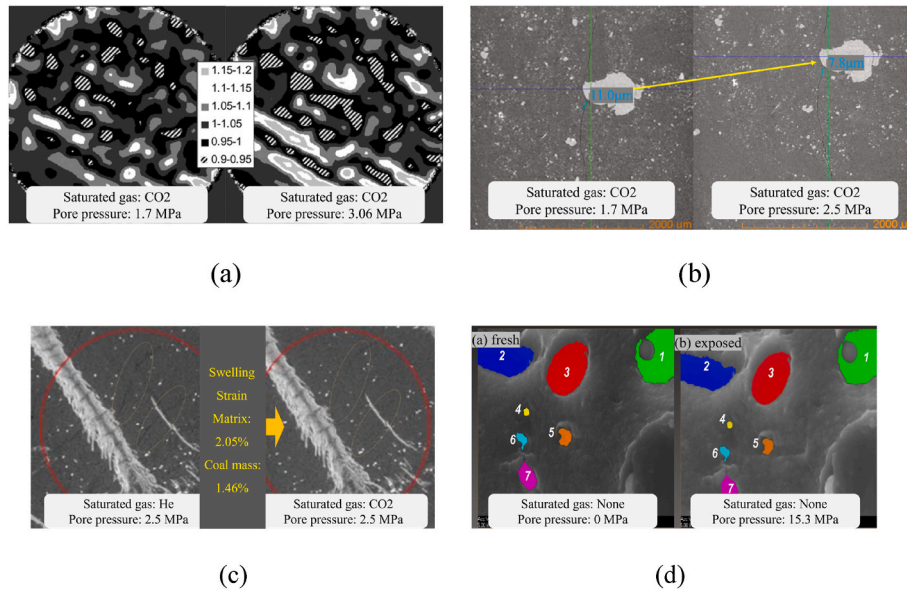


Fig. 1. Evidence of the self-constrained/facilitated swelling cases. (a) non-uniform swelling case [56]; (b) suspected self-constrained swelling case [52]; (c) suspected self-constrained swelling case [59]; (d) suspected self-facilitated swelling case [15].

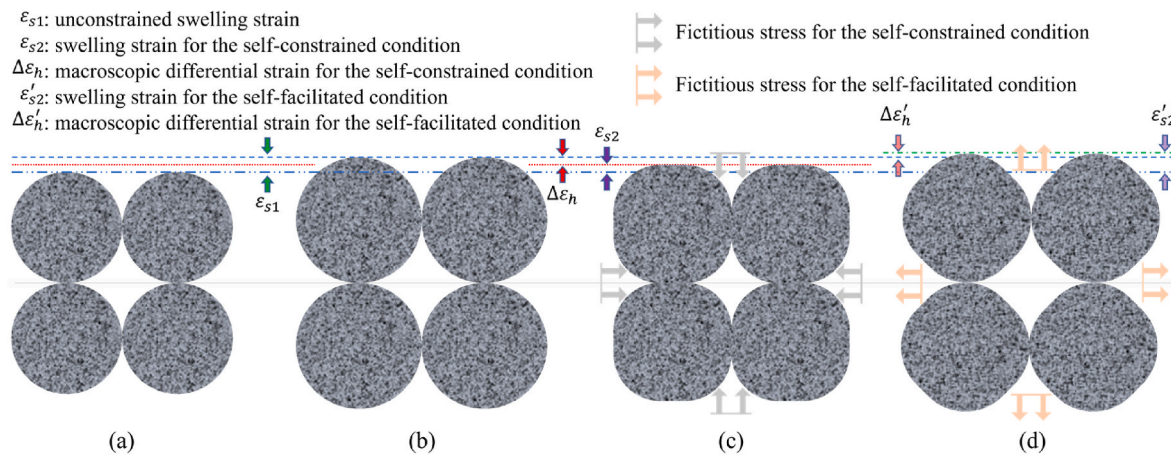


Fig. 2. Illustration of gas adsorption induced internal swelling stress concept. (a) initial equilibrium state; (b) uniform swelling state; (c) self-constrained and (d) self-facilitated adsorption-swelling case, differential strain generated compared with uniform swelling case.

strain for coal mass. Then we have $\epsilon_{s1} = \Delta\epsilon_c^s = \Delta\epsilon_m^s$. By assuming that the adsorption strain of coal matrix in this uniform swelling condition obey the Langmuir type deformation curve [61], the adsorption induced matrix strain can be written as:

$$\Delta\epsilon_m^s = \frac{p * \epsilon_{Lm}}{p + P_{Lm}} - \frac{p_0 * \epsilon_{Lm}}{p_0 + P_{Lm}} \quad (9)$$

Where p is the current gas pressure, p_0 is the initial gas pressure, ϵ_{Lm} and P_{Lm} represent the Langmuir constants for the coal matrix, which can be measured directly in the laboratory by using a small sample containing only matrix [62].

However, as shown in previous CT scans, the uniform swelling state which shown in Fig. 2 (b) may hardly occur due to the interaction between the internal microstructures of coal. In fact, the deformation of coal caused by gas adsorption is a heterogeneous swelling process related to the internal heterogeneous compositions, which may finally present a self-constrained expansion state (Fig. 2 (c)) or even a self-facilitated expansion state (Fig. 2 (d)). Here we use ϵ_{s2} to represent the heterogeneous swelling strain of coal mass, for ease of differentiation, we use ϵ'_{s2} to represent the self-constrained swelling strain and ϵ''_{s2}

to represent the self-facilitated swelling strain. For these two conditions, the corresponding coal mass strain (ϵ_{s2} or ϵ'_{s2}) is the adsorption strain measured at the sample scale [50]. Different from the testing approach of matrix, the adsorption strain at the sample scale is highly heterogeneous, and the self-constrained/facilitated adsorption-swelling behavior is striking. The experimental data show that the adsorption strain of coal mass also currently conforms to the Langmuir form [63]

$$\Delta\epsilon_c^s = \frac{p * \epsilon_{Lc}}{p + P_{Lc}} - \frac{p_0 * \epsilon_{Lc}}{p_0 + P_{Lc}} \quad (10)$$

Where ϵ_{Lc} and P_{Lc} are the Langmuir strain constant and pressure constant, which can be measured directly in laboratory with coal samples.

With the help of micro-CT scan results, we have described this self-constrained/facilitated adsorption-swelling process qualitatively. But quantitatively, it is extremely challenging to quantify the amount of adsorption strain that remains concealed from microstructural observation, owing to the intricate nature of coal structures. Moreover, there is limited literature on the influence of adsorption-induced stress variations resulting from matrix fracture interactions on the change of effective stress. Since the consequence is obvious, where a macroscopic

differential swelling strain exists between complete free and self-constrained condition, as measured before [15,59]. In this research, two different symbols are used to denote the differential strain, $\Delta\epsilon_h$ for the macroscopic differential strain of the self-constrained condition and $\Delta\epsilon'_h$ for the self-facilitated condition. With the previous findings in mind, an alternative approach can be employed to measure the effect of such self-constrained/facilitated adsorption-swelling phenomena. Such a mysterious phenomenon can be considered as a 'fictitious stress' that restricts/promotes the unconstrained uniform swelling of the coal mass. Clearly, for the case of self-constrained adsorption-swelling condition (e.g., Fig. 1(b) and (c)), it can be understood as the existence of a hypothetical force, which we define as the 'fictitious stress' that pushes the coal back from the unconstrained swelling state to its current state, as illustrated in Fig. 2 (c). On the other hand, in the case of self-facilitated adsorption-swelling deformation (as shown in Fig. 1(d)), the effect of this fictitious stress is reversed, as depicted in Fig. 2(d). By assuming that this macroscopic fictitious stress conforms to Hooke's law, the magnitude of the fictitious stress is directly proportional to the magnitude of the differential strain between the uniform swelling case (ϵ_{s1}) and the heterogeneous swelling case (ϵ_{s2}). For the uniform swelling case, as previously mentioned, we have ($\epsilon_{s1} = \Delta\epsilon_c^s = \Delta\epsilon_m^s$), thus (ϵ_{s1}) can be determined through matrix strain measurement, as shown in Eq. (9). For the heterogeneous swelling strain (ϵ_{s2}), it refers to the adsorption strain measured at the sample scale, which is represented by Eq. (10). Thus, the fictitious stress increment $\Delta\sigma_{fic}$ can be expressed as:

$$\Delta\sigma_{fic} = K(\epsilon_{s1} - \epsilon_{s2}) = K(\Delta\epsilon_m^s - \Delta\epsilon_c^s) \quad (11)$$

Where K is the bulk modulus of coal mass, which can be expressed as $K = E/3(1 - 2\nu)$, E is the Young's modulus and ν is the Poisson's ratio. For self-constrained behavior, $\Delta\epsilon_m^s$ is greater than $\Delta\epsilon_c^s$, thus $\Delta\sigma_{fic}$ is greater than 0, indicating compressive stress; for self-facilitated behavior, $\Delta\epsilon_m^s$ is less than $\Delta\epsilon_c^s$, and $\Delta\sigma_{fic}$ is less than 0, indicating tensile stress.

Similarly, we assume that the variations in effective stress resulting from the heterogeneous swelling deformation process of coal samples caused by other physical or chemical property changes (such as thermal related heterogeneous swelling and hygroscopic expansion deformation [32]) can also be addressed by analogy as this self-constrained/facilitated deformation behavior, which is $\Delta\sigma_{fic} = K(\Delta\epsilon_m^t - \Delta\epsilon_c^t)$ and $\Delta\sigma_{fic} = K(\Delta\epsilon_m^h - \Delta\epsilon_c^h)$. Where $\Delta\sigma_{fic}$ represents the fictitious stress increment, $\Delta\epsilon_m^t$ and $\Delta\epsilon_c^t$ are the increments of matrix strain caused by thermal expansion and hygroscopic swelling, $\Delta\epsilon_c^t$ and $\Delta\epsilon_m^h$ are the increments of coal strain caused by thermal expansion and hygroscopic swelling, respectively. Assuming that these three types of fictitious stress can be superimposed on each other, then the fictitious stress can be extended into three types of stress sources.

$$\Delta\sigma_{fic} = K((\Delta\epsilon_m^s - \Delta\epsilon_c^s) + (\Delta\epsilon_m^t - \Delta\epsilon_c^t) + (\Delta\epsilon_m^h - \Delta\epsilon_c^h)) \quad (12)$$

By incorporating Eq. (12) into the conventional Biot effective stress principle, the effect of self-constrained/facilitated adsorption-swelling deformation on the change of effective stress can be explicitly expressed as:

$$\Delta\sigma_e^u = \Delta\sigma_c - \alpha\Delta p + \Delta\sigma_{fic} \quad (13)$$

For ease of reference, in this research we name Eq. (13) as the unconventional effective stress (UES) principle, the effective stress calculated through Eq. (1) and Eq. (2) is named as the conventional effective stress. Apparently, for the assumption of a uniform swelling/shrinking deformation case, gas adsorption or hygroscopic induced coal matrix strain and coal mass strain are same, the fictitious stress vanished and the UES theory degenerated into the conventional effective stress form.

3.3. Fictitious stress dependent permeability models

Through incorporating the fictitious stress concept into the conventional effective stress principle, we have obtained the unconventional one. By substituting Eq. (13) into Eq. (3), a new generic UES-dependent coal permeability model is obtained:

$$\frac{k}{k_0} = \exp(-3c_f(\Delta\sigma_c - \alpha\Delta p + \Delta\sigma_{fic})) \quad (14)$$

When interpreting permeability data measured in the laboratory or in the field, different boundaries are considered. According to the loading mode of coal sample boundary conditions, it can be divided into stress-controlled boundaries (constant confining pressure (CCP), constant Terzaghi effective stress (CTES), constant pore pressure (CP)) and displacement-controlled boundary conditions (constant volume (CV), uniaxial stress (UAS)), the illustration of these boundaries are shown in Fig. 3. To describe the effective stress state and explain the permeability evolution behavior under different boundary conditions, the specific expressions of effective stress under five different boundary conditions are listed and the generic UES-dependent coal permeability model is degenerated into the following boundaries according to the specific loading condition.

(a) Constant confining pressure (CCP) condition

Under the constant confining pressure condition, the increment of the mean confining stress equals to zero.

$$\Delta\sigma_c = 0 \quad (15)$$

Substituting Eq. (15) into Eq. (13), one can obtain the expression for effective stress change under the CCP boundary condition, which is

$$\Delta\sigma_e^u = -\alpha\Delta p + \Delta\sigma_{fic} \quad (16)$$

By submitting Eq. (16) into Eq. (3), one can get the expression of the UES-dependent permeability model for the CCP condition.

$$\frac{k}{k_0} = \exp(-3c_f(-\alpha\Delta p + \Delta\sigma_{fic})) \quad (17)$$

(b) Constant effective stress condition

To distinguish the difference between the conventional effective stress and the current unconventional one, we treat this boundary condition as the constant conventional effective stress (CCES) condition, which is generally named as the constant effective stress (CES) condition in most works [64,65]. Under this condition, the increment of conventional effective stress is equal to zero

$$\Delta\sigma_e = \Delta\sigma_c - \alpha\Delta p = 0 \quad (18)$$

Submitting Eq. (18) into Eq. (13), one can obtain the expression for UES change under the CCES condition.

$$\Delta\sigma_e^u = \Delta\sigma_{fic} \quad (19)$$

The UES dependent permeability model for the CCES boundary can be derived by submitting Eq. (19) into Eq. (3).

$$\frac{k}{k_0} = \exp(-3c_f(\Delta\sigma_{fic})) \quad (20)$$

The CCES boundary is different from other boundaries because the effective stress state is controlled by fictitious stress only, the change of pore pressure caused by gas injection process is considered to offset the change of confining pressure [31]. Considering the influence of hydrostatic confining pressure caused by gas injection under the boundary condition of free expansion (unconstrained expansion), the free swelling boundary belongs to the CCES boundary in essence.

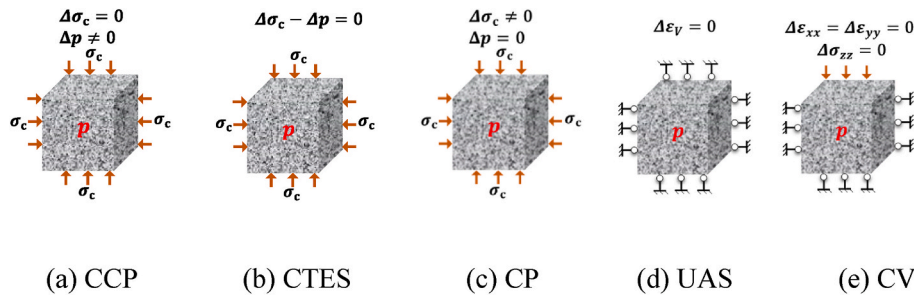


Fig. 3. Schematic diagrams of various boundary conditions: (a) constant confining pressure condition (CCP); (b) constant Terzaghi effective stress condition (CTES); (c) constant pore pressure condition (CP); (d) uniaxial stress condition (UAS); (e) constant volume condition (CV).

(c) Constant pore pressure condition (CP)

Under the constant pore pressure condition, the increment of the pore pressure equals to zero

$$\Delta p = 0 \tag{21}$$

Under this condition, the fictitious stress remains unchanged due to unchanged pore pressure. Thus, the UES is controlled by the confining pressure only

$$\Delta \sigma_e^u = \Delta \sigma_c \tag{22}$$

Then, by submitting Eq. (22) into Eq. (3), one can obtain the UES-dependent permeability model for the CP boundary condition, which is totally controlled by the change of confining pressure.

$$\frac{k}{k_0} = \exp(-3c_f(\Delta \sigma_c)) \tag{23}$$

(d) Uniaxial strain (UAS) condition

Coal reservoirs or sedimentary basins are usually assumed under the uniaxial strain (UAS) condition [33,66]. For the UAS boundary condition, the vertical stress imposed on the coal seam is constant, and zero deformation is allowed in the horizontal directions ($\Delta \epsilon_x = \Delta \epsilon_y = 0$) as shown in Fig. 3 (d). Since the implemented vertical stress is constant $\Delta \sigma_z = 0$, therefore, the effective stress (Here, the effective stress refers to the change in net stress due to boundary loads and pore pressure) change caused by reservoir pressure in the z direction is: $\Delta \sigma_{ez} = -\alpha \Delta p$. Although we have proposed the concept of fictitious stress from the perspective of micro heterogeneity of reservoirs, we assume that the reservoir is isotropic at the macro scale. Assuming gas adsorption induced coal mass strain is same in 3 directions: $\Delta \epsilon_s^{cx} = \Delta \epsilon_s^{cy} = \Delta \epsilon_s^{cz} = \Delta \epsilon_s^c/3$. Thus, coal mass strain in the horizontal direction can be written as

$$\Delta \epsilon_x = \frac{\Delta \sigma_{ex} - \nu \Delta \sigma_{ey} - \nu \Delta \sigma_{ez} - \Delta \epsilon_s^c}{E} \tag{24}$$

$$\Delta \epsilon_y = \frac{\Delta \sigma_{ey} - \nu \Delta \sigma_{ex} - \nu \Delta \sigma_{ez} - \Delta \epsilon_s^c}{E} \tag{25}$$

According to $\Delta \epsilon_x = \Delta \epsilon_y = 0$, $\Delta \sigma_{ez} = -\alpha \Delta p$, one can derive that

$$\Delta \sigma_{ex} = \Delta \sigma_{ey} = -\frac{\nu}{1-\nu} \alpha \Delta p + \frac{E}{3(1-\nu)} \Delta \epsilon_s^c \tag{26}$$

The variation of effective stress in the horizontal direction is a result of changes in pore pressure during the gas injection process, along with the horizontal confining pressure applied to restrain the expansion of the coal mass [26]. However, the self-constrained/facilitated behaviors resulting from the microscopical structure are not accounted for. In the previous section, we introduced the concept of fictitious stress, which is a property related to the change of state of a coal sample, independent of the boundary conditions. Thus, by incorporating fictitious stress term,

the unconventional effective stress of a coal sample under UAS condition can be expressed as

$$\Delta \sigma_e^u = \frac{1}{3} (\Delta \sigma_{ex} + \Delta \sigma_{ey} + \Delta \sigma_{ez} + 3 \Delta \sigma_{fic}) \tag{27}$$

Assuming the change of fictitious stress is the same in three directions, by substituting $\Delta \sigma_{ez} = -\alpha \Delta p$ and Eq. (26) into Eq. (27) yields

$$\Delta \sigma_e^u = -\frac{1+\nu}{3(1-\nu)} \alpha \Delta p + \frac{2E \Delta \epsilon_s^c}{9(1-\nu)} + \Delta \sigma_{fic} \tag{28}$$

One can obtain the UES-dependent permeability model under UAS boundaries by submitting Eq. (28) into Eq. (3)

$$\frac{k}{k_0} = \exp\left(-3c_f\left(-\frac{1+\nu}{3(1-\nu)} \alpha \Delta p + \frac{2E \Delta \epsilon_s^c}{9(1-\nu)} + \Delta \sigma_{fic}\right)\right) \tag{29}$$

(e) Constant volume (CV) condition

For the CV conditions, the displacement of coal sample in each direction is zero, i.e., the total volume of coal mass remains unchanged. The volumetric strain of coal mass can be expressed as:

$$\Delta \epsilon_v = \frac{\Delta \sigma_c - \alpha \Delta p}{K} - \Delta \epsilon_s = 0 \tag{30}$$

Rearranging Eq. (30), we have $\Delta \sigma_c = \alpha \Delta p + K * \Delta \epsilon_s$. This equation represents the magnitude of the confining pressure applied to maintain zero volumetric strain in the coal sample under the combined influence of pore pressure and adsorption. Clearly, this confining pressure loading process will be adjusted correspondingly with changes in pressure. Submitting $\Delta \sigma_c = \alpha \Delta p + K * \Delta \epsilon_s$ into Eq. (13), one can obtain the expression for UES change under the CV condition.

$$\Delta \sigma_e^u = K * \Delta \epsilon_s + \Delta \sigma_{fic} \tag{31}$$

The UES dependent permeability model for the CV boundary can be derived by submitting Eq. (31) into Eq. (3)

$$\frac{k}{k_0} = \exp(-3c_f(K * \Delta \epsilon_s + \Delta \sigma_{fic})) \tag{32}$$

The difference between this UES theory and the exist “back compaction” theory [67] or the similar “push back” theory [61] should be pointed out, in addition to considering the adsorption expansion deformation of the completely bound part, this research also consider the influence of fictitious stress.

4. Model validation

To demonstrate the applicability of the UES-dependent permeability models, we validated the permeability data from stress-controlled boundary conditions and displacement-controlled boundary conditions, respectively in this section. The data of the stress-controlled boundary conditions are derived from the CCP boundary condition

[68], and the corresponding UES permeability model is Eq. (17); the data of the displacement-controlled boundary conditions are derived from the UAS boundary conditions [69]. Meanwhile, the evolution trend of the unconventional effective stress within these coal samples under different equilibrium pressures was also estimated and illustrated. These experiments were performed under isothermal conditions, so fictitious stress is only due to adsorption. Biot coefficient is assumed to be unity for both validation processes [33].

4.1. Stress controlled boundary

The permeability data provided by Ref. [68] was used for verification, which was tested under the constant confining pressure condition. Under stress-controlled boundary conditions, due to the absence of displacement constraints, coal volumetric expansion is unrestricted. Under constant confining pressure boundary conditions, as the boundary load remains fixed, according to Eq. (17), changes in permeability are jointly controlled by variations in pore pressure ($-\alpha\Delta p$) and changes in fictitious stress ($\Delta\sigma_{fic}$). During the gas injection process, with increasing gas pressure, the term ($-\alpha\Delta p$) assumes negative values, resulting in an increase in permeability.

The influence of fictitious stress varies with the coal sample. According to the definition, when the sample exhibits self-constrained behavior ($\Delta\sigma_{fic} > 0$), leading to a decrease in permeability it competes with the effect of pore pressure at this point. When the sample exhibits self-facilitated behavior ($\Delta\sigma_{fic} < 0$), it leads to an increase in permeability, same effect as pore pressure. However, when ($\Delta\sigma_{fic} = 0$), adsorption does not impact permeability changes.

The parameters used are listed in Table 1, it should be noted that the Langmuir adsorption constants for the coal matrix were not tested in their research, we obtained by matching the experimental data. Furthermore, based on specific coal parameters, this study conducts a comparative analysis of three different expressions of effective stress, namely UES, CES, and $CES + K * \Delta\epsilon_s^c$, as illustrated in Fig. 4(b).

From Fig. 4 (a), we can see that the UES-dependent permeability model fits well with the data for the Anderson coal, indicating that it can be used to predict the permeability evolution under CCP condition and other stress-controlled boundary conditions. It should be noted that we also compared the performance of our UES-dependent permeability model with the other permeability models based on the conventional effective stress theory. The CES-dependent model refers to the direct use of the conventional effective stress to explain the evolutionary trend of the permeability, which is achieved by substituting Eq. (2) into Eq. (3). While the $CES + K * \Delta\epsilon_s^c$ -dependent permeability model refers to the integration of the adsorption stress obtained from the calculation method of specific thermal expansion stress into the traditional effective stress treatment method, which can be expressed by substituting Eq. (5) into Eq. (3). The $CES + f * K * \Delta\epsilon_s^c$ -dependent model refers to the separating adsorption stress approach, which can be expressed by substituting Eq. (6) into Eq. (3).

The matching results suggest that the UES-dependent model can make a better description of the processes. Obviously, the $CES + K * \Delta\epsilon_s^c$ based theory predicts a lower trend, which is because all the swelling deformation assumed to be constrained and it is converted into

adsorption stress. As a result, this treatment makes the effect of adsorption on effective stress significantly overestimated, as shown in Fig. 4 (b). When $f = 0.45$, the $CES + f * K * \Delta\epsilon_s^c$ based approach can fit to the first point, but still fails to explain the overall data. The CES-dependent permeability model predicts a higher evolutionary trend due to an underestimation of the effect of adsorption caused by the absence of the adsorption stress term. Correspondingly, the effective stress based on various theories is depicted in Fig. 4 (b). It is observed that the initial increase and subsequent decrease of UES with pore pressure is the fundamental reason for the observed increase followed by a decrease in permeability.

4.2. Displacement controlled boundary

Under the UAS boundary condition, the UES-dependent permeability model is expressed in Eq. (29), the expression of UES is Eq. (28). Under displacement-controlled boundary conditions, the adsorption-induced deformation of coal samples is partially restricted (UAS boundary, horizontal constraint) or entirely constrained (CV boundary). During this scenario, the adsorption effect partially or fully contributes to the variations in effective stress, subsequently influencing the evolution of permeability, e.g., $\frac{2E\Delta\epsilon_s^c}{9(1-\nu)}$ in Eqs. (28) and (29). Additionally, similar to the stress-controlled boundary conditions, it is also influenced by changes in pore pressure and variations in fictitious stress. Excluding the fictitious stress term, Eq. (28) is degraded into to formation used in Refs. [26,71] for calculating effective stress. The laboratory tested permeability data [69], which was conducted under the UAS boundary condition, is used here for validating the UES-dependent permeability model. The input parameters for the fitting process are listed in Table 2, these parameters are acquired from published literatures [33,72,73]. It should also be noted that the S&D permeability model [26] derived based on uniaxial strain boundary conditions and the modified one [73] were used here for comparative analysis. The model fitting results and comparative analysis for different effective stresses can be found in Fig. 5.

The fitting results and the UES evolution with pore pressure are depicted in Fig. 5 (a). The UES-dependent model fits well with the testing data, indicating that the model can be used to predict the permeability evolution of the coal samples under UAS boundary and can also be popularized to predict gas production on site, since a UAS boundary is usually assumed to represent the reservoir boundary [74]. Whereas, when compared to the S&D model, the modified version incorporates a slightly larger coefficient to account for the influence of adsorption-induced strain. When analyzing the red and green lines in Fig. 5(b), it becomes apparent that the modified version showcases a more pronounced manifestation of the effects of adsorption. Although this adjustment brings the model's curve closer to explaining experimental data, a slight disparity remains. Compared with the classical S&D permeability model, the modified one or other permeability models applicable to uniaxial strain boundary conditions [62,71], the UES with the addition of fictitious stress can better reflect the actual stress state of the reservoir, and the UES-dependent permeability model can better depict the reservoir permeability evolution trend.

5. Discussions

By incorporating the fictitious stress term (which can represent the self-constrained/self-facilitated behavior of coal adsorption deformation), we have extended the conventional effective stress principle to an unconventional one. Next, we will discuss the relations and differences between the two as well as conduct a preliminary analysis of the approximate application of unconventional effective stress.

Table 1
Parameters for data matching under stress controlled boundary condition [68,70].

Parameter	Value
Bulk modulus, K (MPa)	1356
Fracture compressibility, c_f (MPa^{-1})	0.058
Langmuir strain of coal mass, ϵ_{Lc}	0.035
Langmuir pressure of coal mass, P_{Lc} (MPa)	3.5
Langmuir strain of coal matrix, ϵ_{Lm}	0.041
Langmuir pressure of coal matrix, P_{Lm} (MPa)	2.3

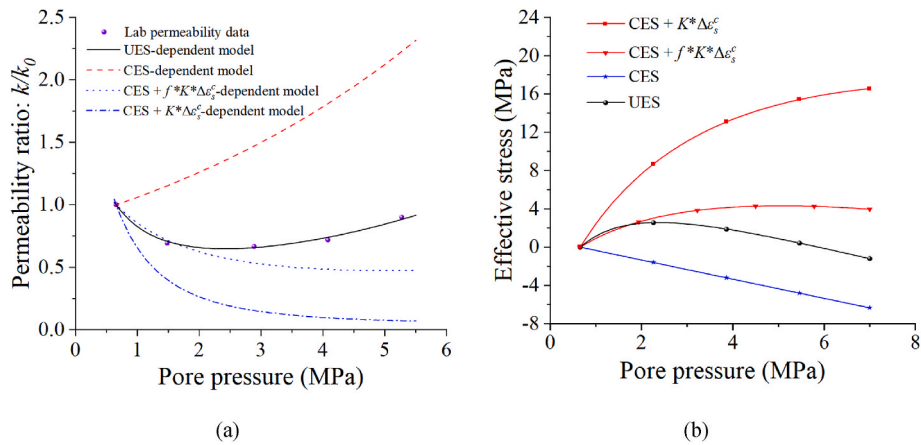


Fig. 4. Matching results under constant confining pressure condition: (a) modeled results with tested data (b) estimated effective stress with pore pressure.

Table 2
Parameters for data matching under UAS conditions.

Parameter	Value
Young's modulus, E (MPa)	1713
Poisson's ratio, ν	0.35
Fracture compressibility, c_f (MPa ⁻¹)	0.078
Langmuir strain of coal mass, ϵ_{Lc}	0.01075
Langmuir pressure of coal mass, P_{Lc} (MPa)	4.16
Langmuir strain of coal matrix, ϵ_{Lm}	0.019
Langmuir pressure of coal matrix, P_{Lm} (MPa)	2.95

5.1. Contrast analysis between the CES and the UES

The UES-dependent model, in the previous model validation process, has shown the accuracy of depicting the trend of permeability data changes.

The existence of fictitious stress term distinguishes the CES principle and the UES principle, we can find this difference by comparing Eq. (2) with Eq. (13). By substituting Eq. (2) and Eq. (13) into Eq. (3), one can obtain permeability models controlled by the CES theory and the UES theory, respectively. Based on the data provided in Table 1, the permeability evolution data estimated by these two models can be obtained, as shown in Fig. 6. The prediction results of UES-dependent model are consistent with the general trend of permeability data [31].

On the other hand, the impact of self-constrained or self-facilitated adsorption-swelling deformation on reservoir permeability can be offset by adjusting the confining pressure. For the data shown in Fig. 6, for example, the fictitious stress is above 0 represents a self-constraint

swelling occurs inside, then the permeability of any test point can be brought back to the original value by reducing the corresponding confining pressure, vice versa.

The difference between the CES principle and the UES principle also raises another issue. When investigating how the permeability changes with the variation of effective stress, there are different loading paths to choose [75]. One can choose to keep the pore pressure unchanged and adjust the confining pressure (as shown in Table 3, loading path 1) [64], or the pore pressure and confining pressure adopt different gradient loading (by assuming α equals to unity, as shown in Table 3, loading path 2 and 3) [76]. The three effective stress loading paths are visually

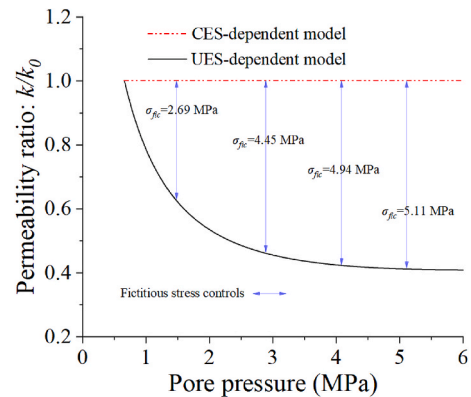


Fig. 6. Comparison between CES and UES: the role of fictitious stress.

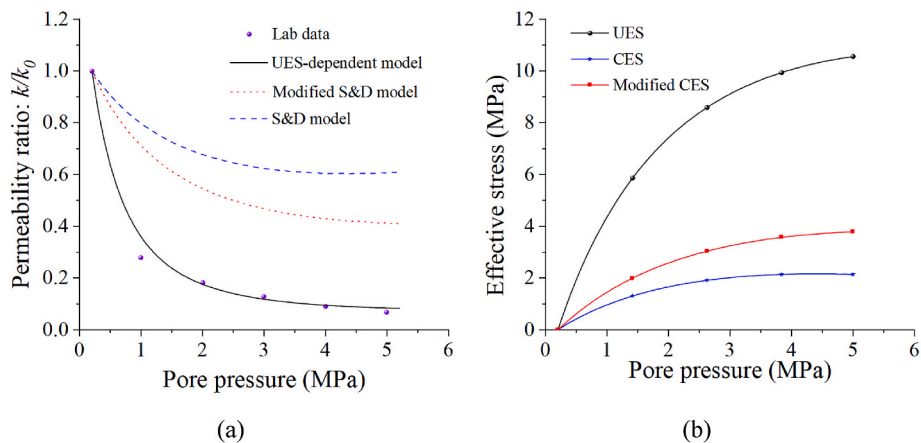


Fig. 5. Matching results under uniaxial strain condition: (a) modeled results with tested data (b) estimated effective stress with pore pressure.

Table 3
Different loading paths for the same effective stress gradient (by assuming Biot's coefficient α equals to unity).

Terzaghi effective stress, MPa		0	1	2	3	4	5	6
Loading path 1	p, MPa	1	1	1	1	1	1	1
	σ_c, MPa	1	2	3	4	5	6	7
Loading path 2	p, MPa	0	1	2	3	4	5	6
	σ_c, MPa	0	2	4	6	8	10	12
Loading path 3	p, MPa	0	2	4	6	8	10	12
	σ_c, MPa	0	3	6	9	12	15	18

depicted in Fig. 7 (a). From this, we can observe that three different loading paths can lead to the same loading gradient in conventional effective stress.

The first loading path, in essence, is the CP (constant pore pressure, confining pressure changes) condition. As the pore pressure remains unchanged, adsorption will hardly affect the permeability evolution as reported in the experimental work [59]. The fictitious stress disappears in this case, the UES degraded into the conventional form. As indicated in Eq. (22) and Eq. (23), the variation of effective stress and permeability are controlled by confining pressure only, as shown in Fig. 7 (b). However, for loading path 2 and 3, the simultaneously changed pore pressure and confining pressure can lead to different results. Although the loading gradient of effective stress in loading paths 2 and 3 are the same as that of the first loading path, the fictitious stress will gradually increase with the increase of pore pressure. Under such circumstances, the changeable fictitious stress makes the difference between unconventional effective stress and the conventional Terzaghi effective stress, and further affects the evolution of permeability as illustrated in Fig. 7 (b).

5.2. Effect of various coal adsorption properties

The concept of fictitious stress is a characterization of the self-constrained/facilitated adsorption-swelling behavior controlled by the internal structure of coal. The difference between the Langmuir adsorption constants of coal matrix and coal mass leads to the origin of the self-constraint or self-facilitated adsorption-swelling behavior and thus the fictitious stress. Gas adsorption can result in coal volumetric swelling strain of up to 5 % or even more [48], while typical Langmuir adsorption pressure can range from a few kilopascals to several tens of megapascals [62]. To explore what parameter combinations can represent self-constrained behavior or self-facilitated adsorption-swelling behavior, we investigated 9 cases regarding the relative size relationship between the adsorption constant of coal matrix and coal mass. Among them, the case with $P_{Lc} = P_{Lm} = 3MPa$, $\epsilon_{Lc} = \epsilon_{Lm} = 0.04$ is taken as the intermediate case. Then, the relative sizes of the parameters are

adjusted. These 9 cases cover all the theoretically possible relative size relationships, which allows our findings to be generalized to general applications. Nine sets of parameters are shown in Table 4, based on which we will explore the effects of these combinations on fictitious stress, permeability evolution, and unconventional effective stresses at sample scale.

5.2.1. Effect on fictitious stress

According to Eq. (9)-Eq. (11), we simulated the variation of fictitious stress with pore pressure for 9 different cases, as shown in Fig. 8. Coal matrix and coal mass share the same Langmuir adsorption strain constant and pressure constant for case 5, a uniform swelling behavior rather than self-constraint/facilitated swelling occurs with the increase of pore pressure, and the fictitious stress remains zero. Among them, case 5 divides the data into two regions. The fictitious stress in the area above the case 5 curve is greater than 0, indicating self-constraint adsorption-swelling behavior, and the fictitious stress below the case 5 curve is less than 0, indicating self-facilitated behavior. In Langmuir theory, the adsorption strain constant is the maximum adsorption strain when the pressure reaches infinity; the adsorption pressure constant is the pressure corresponding to half of the maximum adsorption strain, the adsorption strain constant determines the final value of the Langmuir adsorption curve while the Langmuir adsorption pressure constant determines the steepness of the adsorption curve.

When P_{Lc} and P_{Lm} remained unchanged (comparing case 1,2,3 or 4,5,6 or 7,8,9), the trend of fictitious stress is controlled by the relative magnitude of ϵ_{Lm} and ϵ_{Lc} . When $P_{Lc} > P_{Lm}$ and $\epsilon_{Lc} < \epsilon_{Lm}$ (case 1), it can be observed that with an increase in pore pressure, the fictitious stress is greater than zero and monotonically increases. This indicates the occurrence of self-constrained adsorption-swelling behavior exclusively. Conversely, when $P_{Lc} < P_{Lm}$ and $\epsilon_{Lc} > \epsilon_{Lm}$ (case 9), with an increase in pore pressure, the fictitious stress is less than zero and monotonically decreases, which directing the self-facilitated adsorption-swelling behavior. However, when $P_{Lc} > P_{Lm}$ and $\epsilon_{Lc} \geq \epsilon_{Lm}$ (case 2, 3), or $P_{Lc} < P_{Lm}$ and $\epsilon_{Lc} \leq \epsilon_{Lm}$ (case 7, 8), the fictitious stress exhibits a turning phenomenon. In case 3, when $P_{Lc} < P_{Lm}$; $\epsilon_{Lc} > \epsilon_{Lm}$, or in case 7, when $P_{Lc} > P_{Lm}$; $\epsilon_{Lc} < \epsilon_{Lm}$, the fictitious stress curve undergoes a significant inflection that crosses the coordinate axis. This indicates a transition in the adsorption-induced expansion behavior of the sample. For example, in case 3, the behavior transitions from self-constrained behavior to self-facilitated behavior, while in case 7, it transitions from self-facilitated behavior to self-constrained behavior. When $P_{Lc} = P_{Lm}$ (case 4, 5, 6), the relative magnitudes of ϵ_{Lc} and ϵ_{Lm} determine the monotonic trend of fictitious stress and the adsorption behavior as follows: case 4: $\epsilon_{Lc} < \epsilon_{Lm}$, self-constrained swelling; case 5: $\epsilon_{Lc} = \epsilon_{Lm}$, uniform swelling; case 6: $\epsilon_{Lc} > \epsilon_{Lm}$, self-facilitated swelling. In the cases where $\epsilon_{Lc} = \epsilon_{Lm}$ (case 2, 5, 8), despite being influenced differently by P_{Lc} and P_{Lm} , according to

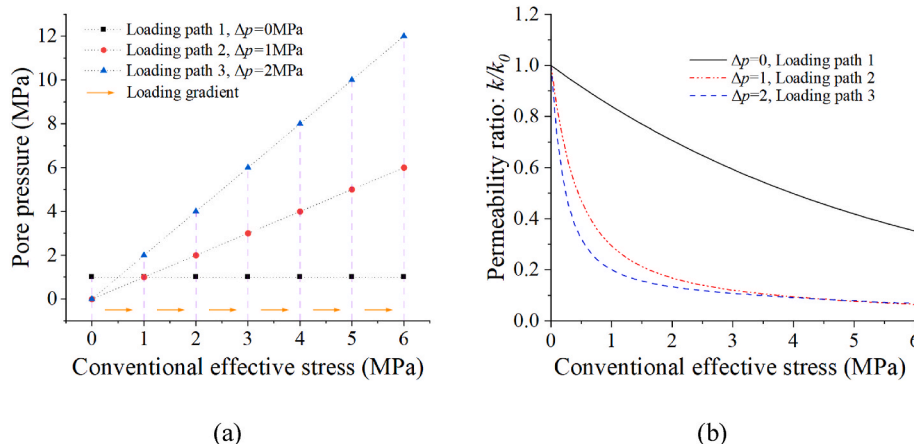


Fig. 7. Effect of different effective stress loading paths.

Table 4

Langmuir constants of coal mass (P_{Lc} : Langmuir pressure constant, ϵ_{Lc} : Langmuir pressure constant) and matrix (P_{Lm} : Langmuir pressure constant, ϵ_{Lm} : Langmuir pressure constant) for 9 cases.

Case number	1	2	3	4	5	6	7	8	9
ϵ_{Lc}	0.04	0.04	0.04	0.04	0.04	0.04	0.04	0.04	0.04
P_{Lc} , MPa	4	4	4	3	3	3	2	2	2
ϵ_{Lm}	0.045	0.04	0.035	0.045	0.04	0.035	0.045	0.04	0.035
P_{Lm} , MPa	3	3	3	3	3	3	3	3	3

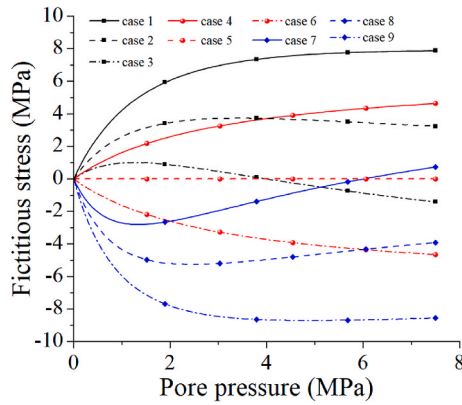


Fig. 8. Fictitious stress for 9 coal sample cases with different adsorption parameters.

the definition of fictitious stress and Langmuir function, when the pressure reaches a sufficiently high level, the final values of fictitious stress for case 2, 5, and 8 are the same.

5.2.2. Effect on permeability

In this section, we will evaluate the effect of different fictitious stress on the evolution of permeability. The assessment background is based on the constant Terzaghi effective stress boundary since permeability is controlled by fictitious stress only at this condition according to Eq. (20). The evaluation results for 9 cases are shown in Fig. 9. Normally, according to the statistics, the experimental data under the constant Terzaghi effective stress gradually decreases with the increase of pore pressure [31]. The results of cases 1-5, 7 generally align with the predicted results from statistical data. However, Case 6, 8, and 9 deviate significantly from the data within the statistical range, which indicates that the adsorption-induced expansion behavior corresponding to Cases 6, 8, and 9 may actually occur infrequently or rarely in practice.

5.2.3. Effect on unconventional effective stress

By incorporating the fictitious stress concept into the conventional

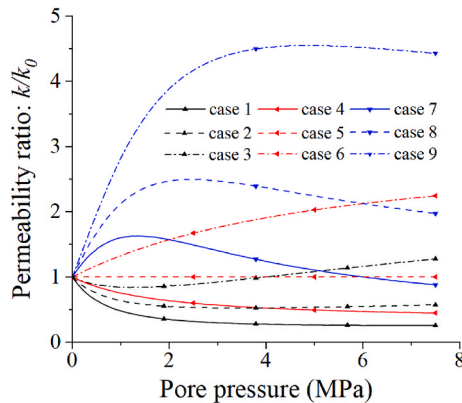


Fig. 9. The influence of fictitious stress on the evolution of permeability.

effective stress principle, we have obtained the unconventional one (UES). Considering the confining pressure loading under different boundary conditions, we have derived expressions for unconventional effective stress under five different boundary conditions. Previously, we investigated the evolutionary trends of fictitious stress in various adsorption parameter cases. In this section, we will further evaluate the trends of the UES of 9 cases under different boundary conditions during the gas injection process. It should be noted that the adsorption constants used in the evaluation process are obtained from Table 4, while the remaining parameters are sourced from Table 2.

For the constant Terzaghi effective stress condition, which we called as the constant conventional effective stress condition (CCES), the UES is controlled by fictitious stress only according to Eq. (19), the UES at this point corresponds to the content depicted in Fig. 8. Based on Eq. (16), we investigated the variation of UES with increasing injection pressure under the CCP boundary, as depicted in Fig. 10. From the graph, it can be observed that all 9 cases exhibit a decrease in the curves in the later stages. Case 5 represents the variation of effective stress under the CCP boundary condition without considering the influence of adsorption. Based on Case 5, we can observe the variations of UES under different fictitious stress conditions. In Cases 1, 2, 3, and 4, the curves show a phenomenon of initially increasing and then decreasing. This is because the UES is influenced not only by fictitious stress but also by the control of pore pressure. The combined effect of these two factors determines the trend of the curves. As for the constant pore pressure condition, since the fictitious stress keeps unchanged, the UES is controlled by loading pressure only.

The evolution of UES corresponding to the nine cases under the uniaxial strain (UAS) boundary condition is shown in Fig. 11. For the nine cases, each exhibits a phenomenon where the UES increases with the rise in pore pressure, which differs from the stress-controlled boundary condition (see Fig. 10). According to the expression for UES under the UAS boundary condition (Eq. (28)), the three terms on the right-hand side determine its evolution. Where, the first term ($-\frac{1+\nu}{3(1-\nu)}\alpha\Delta p$) represents the influence of changes in pore pressure, the second term ($+\frac{2E\Delta\epsilon_c}{9(1-\nu)}$) signifies the effects when adsorption strain is laterally constrained, and the third term ($+\Delta\sigma_{fic}$) denotes the influence of fictitious stress. Given that the Poisson's ratio typically ranges

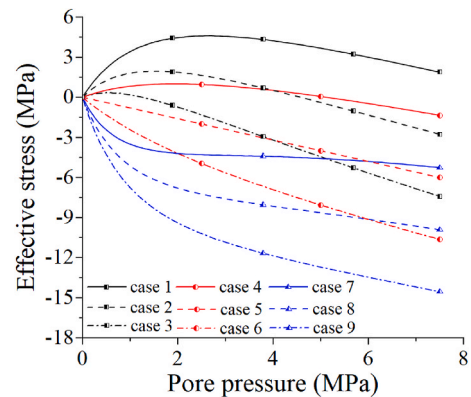


Fig. 10. Evolution of UES under the boundary of CCP.

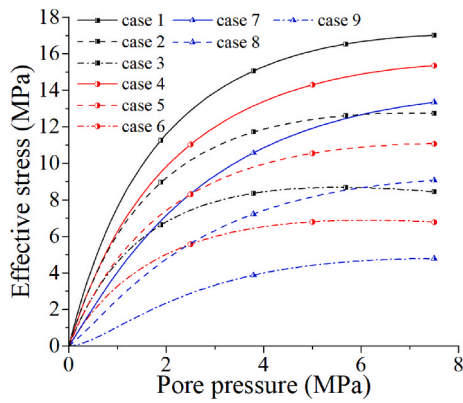


Fig. 11. Evolution of UES under the boundary of UAS.

between 0 and 0.5 [77], and that both Biot’s coefficient and Young’s modulus are non-negative, the following implications arise: As pore pressure increases, the first term remains negative and continues to decrease. The second term, correlated positively with the Langmuir adsorption strain, increasing with rising pressure and finally stabilizes [29]. The fictitious stress is positive for a self-constrained case and negative for a self-facilitated case as indicated in Fig. 8. Therefore, under the UAS boundary condition, the increase of UES due to the constraint of adsorption strain in the horizontal direction ($+\frac{2E\Delta\epsilon_c^c}{9(1-\nu)}$) is greater than the

effects of the other two terms ($-\frac{1+\nu}{3(1-\nu)}\alpha\Delta p, +\Delta\sigma_{fic}$), leading to an observed increase in UES. Moreover, as the effect of adsorption ultimately stabilizes, when the pressure becomes extremely high, terms ($+\frac{2E\Delta\epsilon_c^c}{9(1-\nu)}$) and ($+\Delta\sigma_{fic}$) will remain almost unchanged, and under the influence of term ($-\frac{1+\nu}{3(1-\nu)}\alpha\Delta p$), the UES will ultimately decrease.

5.3. Approximate analysis of stress state evolution during gas storage process

During underground gas storage operations, the stress conditions within an unconventional reservoir undergo dynamic alterations due to variations in pore pressure and gas adsorption. A Mohr’s diagram analysis is often used to depict the stress state in rock formations [78, 79]. Assuming the reservoir is under UAS boundary conditions, it is considered that the diameter and center position of the Mohr circle are related to the effective stresses in both the vertical (σ_v^e) and horizontal (σ_h^e) directions [74,80]. In a Cartesian coordinate system, the radius and center position of the Mohr circle can be represented as follows [74]:

$$R = \frac{\sigma_v^e - \sigma_h^e}{2} \tag{33}$$

$$O = \sigma_h^e + R \tag{34}$$

Where R is the radius of the Mohr’s circle, O is the center coordinate of the Mohr’s circle. Assuming that the initial vertical effective stress (σ_v^{e0})

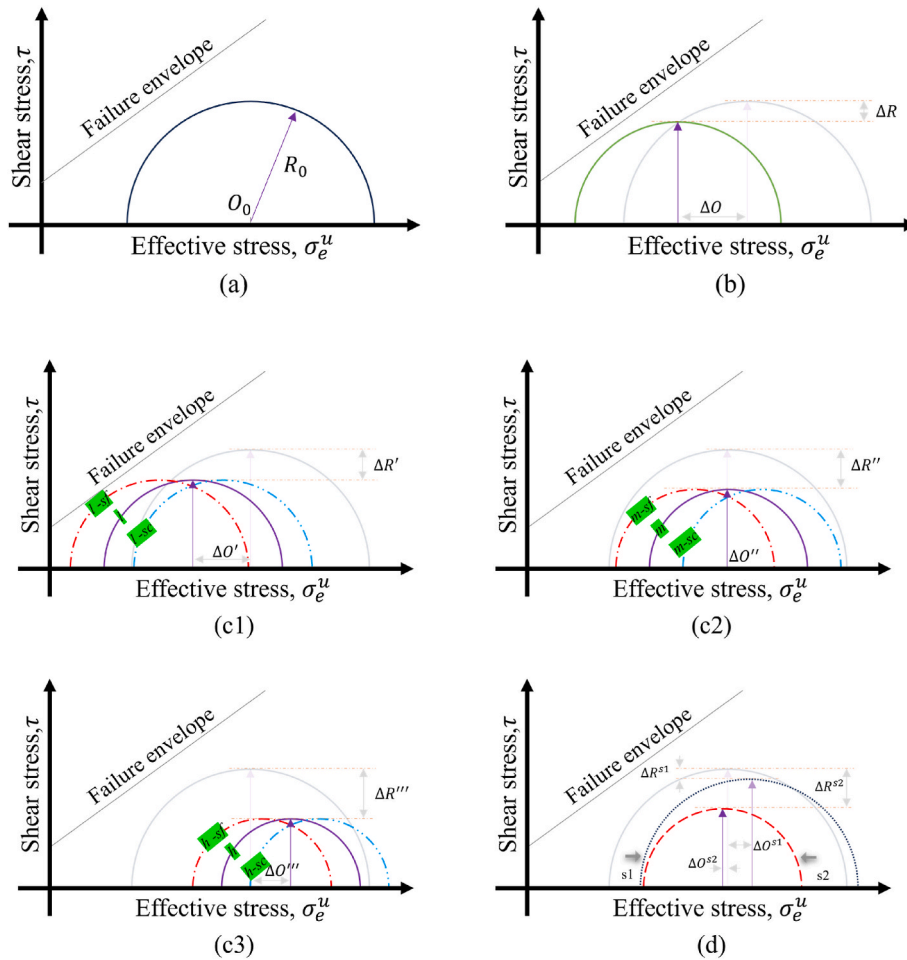


Fig. 12. Schematic diagrams of the state of reservoir stress evolution with gas injection: (a) initial stress state; (b) without gas adsorption effect; (c1,c2,c3) with gas adsorption effect: (c1) lower adsorption ability; (c2) medium adsorption ability; (c3) higher adsorption ability. (d) dynamic evolution of reservoir stress state during gas injection process.

and horizontal effective stress (σ_h^e) are known, the initial center position O_0 and initial radius R_0 of the Mohr circle can be represented according to Eqs. (33) and (34)

$$\Delta R = \frac{\Delta\sigma_v^e - \Delta\sigma_h^e}{2} \quad (35)$$

$$\Delta O = \Delta\sigma_h^e + \Delta R \quad (36)$$

Supposing that the Mohr circle drawn based on the initial center and radius is depicted in Fig. 12 (a), where the horizontal axis represents the normal effective stress, and the vertical axis represents the shear stress. The Mohr-Coulomb criterion has been effectively utilized for the determination of shear failure of brittle rocks such as coal which is a function of the apparent cohesion and the angle of internal friction [74]. In this research, we assume that the coal's failure envelope follows a linear pattern and stays constant as gas injected, as illustrated in Fig. 12. The failure envelope defines the maximum shear stress that a coal can sustain as a function of normal effective stress. When the Mohr's circle touches the failure envelope, the coal fails by shearing. Clearly, as the gas injection process progresses and pressure changes, the effects of pressure change and adsorption will inevitably alter both axial and lateral effective stresses, leading to corresponding changes in the Mohr's circles.

Comparing Eqs. 35 and 36 with Eqs. 33 and 34, correspondingly, the changes in Mohr circle radius and center position can be represented as follows:

$$\Delta R = R - R_0 = \frac{\Delta\sigma_v^e - \Delta\sigma_h^e}{2} \quad (37)$$

$$\Delta O = O - O_0 = \Delta\sigma_h^e + \Delta R \quad (38)$$

Where $\Delta\sigma_v^e$ represents the change in vertical effective stress, and $\Delta\sigma_h^e$ represents the change in horizontal effective stress. According to the unconventional effective stress principle proposed in this study, the vertical effective stress under UAS boundary conditions can be obtained by substituting $\Delta\sigma_{ez} = -\alpha\Delta p$ into Eq. (13), which is

$$\Delta\sigma_v^e = -\alpha\Delta p + \Delta\sigma_{fic} \quad (39)$$

Similarly, the change in horizontal effective stress can ultimately be represented as:

$$\Delta\sigma_h^e = -\frac{\nu}{1-\nu}\alpha\Delta p + \frac{E}{3(1-\nu)}\Delta\epsilon_s^e + \Delta\sigma_{fic} \quad (40)$$

Substituting Eqs. (39) and (40) into Eqs. (37) and (38), we can derive the expressions for the change in Mohr circle radius and the shift in its center position

$$\Delta R = -\frac{1-2\nu}{2(1-\nu)}\alpha\Delta p - \frac{E}{6(1-\nu)}\Delta\epsilon_s^e \quad (41)$$

$$\Delta O = -\frac{1}{2(1-\nu)}\alpha\Delta p + \frac{E}{6(1-\nu)}\Delta\epsilon_s^e + \Delta\sigma_{fic} \quad (42)$$

The change in the radius of the Mohr circle is influenced by both pressure variations and adsorption-induced strain, as the impact of fictitious stress is nullified in both the horizontal and axial directions, as seen in Eqs. (37), (39) and (40).

During the gas storage process, variations in gas pressure, coupled with the effects of constrained horizontal adsorption deformation and the influence of self-constrained/self-facilitated behavior in the form of fictitious stress, collectively determine the evolution of stress states. By considering the initial stress state and pressure changes, we can determine the stress state and Mohr's circles at a specific moment. In this section, we will conduct a qualitative analysis of the influences of different factors on various aspects of this topic. If we assume that the adsorption of the stored gas has no impact on coal volume deformation, such as in the case of hydrogen [22], then in Eqs. (41) and (42), only the

first term on the right-hand side will be effective. Consequently, the changes in the radius and center position of the Mohr's circle will be solely influenced by pressure variations. Compared to the initial reservoir pressure, the gas storage process inevitably leads to an increase in reservoir pressure, where the term $\alpha\Delta p$ is greater than zero. Normally the Poisson's ratio of coal is between 0 and 0.5 [77], therefore ΔR and ΔO consistently remains less than zero. Accordingly, the Mohr's circle under this condition is depicted in Fig. 12 (b).

When accounting for the influence of gas adsorption, the adsorption strain gradually increases according to the definition of the Langmuir equation, thus $\Delta\epsilon_s^e$ is a non-negative value. Therefore, ΔR consistently remains less than zero. In other words, the size of the Mohr circle continuously decreases. The center shift of the Mohr circle's is collectively controlled by the three terms on the right side of Eq. (42). According to the analysis, during the gas injection process, the first term ($-\frac{1}{2(1-\nu)}\alpha\Delta p$) consistently remains less than zero, exerting a leftward shift on the circle's center. The second term ($+\frac{E}{6(1-\nu)}\Delta\epsilon_s^e$) consistently remains greater than zero, causing a rightward shift in the center, and these two terms compete. To better illustrate this interplay of competing effects, let's first consider the case of uniform expansion, i.e., $\Delta\sigma_{fic} = 0$. We will examine three reservoirs with different adsorption capacities, categorized as low (*l*), medium (*m*), and high (*h*) adsorption abilities. Among these, reservoirs with stronger adsorption correspond to larger $\Delta\epsilon_s^e$. The specific Mohr circles are shown in Fig. 12 c, where c_1, c_2, c_3 correspond to reservoirs with low, medium, and high adsorption ability, respectively. The changes in Mohr circle radius and center position are denoted as $\Delta R', \Delta R'', \Delta R'''$ and $\Delta O', \Delta O'', \Delta O'''$. Based on the previous analysis, it is evident that for reservoirs with high adsorption capacity, under the same pressure drop conditions, the Mohr circle has a smaller radius, and the center position is further to the right. For reservoirs with low adsorption capacity, the trend is the opposite.

As for the third term ($+\Delta\sigma_{fic}$) in Eq. (42), influenced by fictitious stress, is related to the internal structure of the coal. We assume that the self-constrained/facilitated adsorption-swelling behavior may exist in all coal reservoirs. Whereas for a self-constrained coal, fictitious stress will lead to a rightward shift because $\Delta\sigma_{fic} > 0$, the corresponding Mohr circles *l-sc*, *m-sc*, and *h-sc* are shown in Fig. 12 (c1, c2, and c3). While it's the opposite for self-facilitated coal, the corresponding Mohr circles are shown as *l-sf*, *m-sf*, and *h-sf*.

It is evident from the analysis that the Mohr circle radius consistently decreases with a continuous gas storage process due to the increasing pressure. Conversely, the change in the circle's center position exhibits fluctuations. Initially, during the early stages when pressure increments are not substantial, the dominant influence is attributed to adsorption effects, resulting in a rightward shift of the circle's center, as illustrated in Fig. 12 (d), the process labeled as s1. As pressure continues to increase to a certain extent, the impact of adsorption gradually diminishes, and under the influence of pore pressure, the circle's position might shift towards the left, as depicted in Fig. 12 (d), the process denoted as s2. Additionally, the influence of the fictitious stress could lead to both leftward and rightward shifts in the circle's center position. Regarding the s2 stage, the Mohr circle will shift to the left toward to the failure envelope but whether it touches the failure envelope depends on specific reservoir parameters such as adsorption strain, contact angle, internal friction angle [74,79].

6. Conclusions

The fictitious stress concept has been incorporated into the conventional Terzaghi principle. This incorporation has transformed the conventional one into unconventional effective stress principle. The unconventional principle has been applied to model coal permeability behaviors and analyze stress state evolution in reservoirs during gas storage processes.

Based on the model results, the following conclusions can be drawn:

- The structural effects of coal and the heterogeneous effects of gas adsorption induced swelling are responsible for the characteristics of coal permeability behaviors. Their resultant effect may constrain or facilitate coal swelling. The fictitious stress is compressive for the case of self-constrained swelling and extensive for the case of self-facilitated swelling.
- Under displacement-controlled boundary conditions, the influence of coal adsorption deformation comprises two components. Firstly, there is an increase in confining pressure due to the constraint on volume deformation. Secondly, there is an influence from the fictitious stress corresponding to self-constrained or self-facilitated adsorption-swelling deformation. These two components collectively govern the evolution process of coal permeability and stress state.
- The unconventional effective stress principle can characterize coal permeability and stress behaviors well. More importantly, coal stress state and permeability evolution are uniquely defined by unconventional effective stresses.

Declaration of competing interest

The authors declare that they have no known competing financial interests or personal relationships that could have appeared to influence the work reported in this paper.

Acknowledgements

This work is supported by the Australian Research Council under Grant DP200101293, the first author is supported by the UWA-China joint scholarships. These sources of support are gratefully acknowledged.

References

- Chen L, Msigwa G, Yang M, Osman AI, Fawzy S, Rooney DW, et al. Strategies to achieve a carbon neutral society: a review. *Environ Chem Lett* 2022;20:2277–310.
- Camargo JT, White JA, Hamon FP, Fakeye V, Buscheck TA, Huerta N. Managing reservoir dynamics when converting natural gas fields to underground hydrogen storage. *Int J Hydrogen Energy* 2024;49:1261–73.
- Sari E, Çiftçi E. A numerical investigation on the utilization of a depleted natural gas field for seasonal hydrogen storage: a case study for Değirmenköy gas field. *Int J Hydrogen Energy* 2024;51:219–28.
- Liu Z, Deng Z, He G, Wang H, Zhang X, Lin J, et al. Challenges and opportunities for carbon neutrality in China. *Nat Rev Earth Environ* 2021;3:141–55.
- P K WG, R PG. An overview of underground hydrogen storage with prospects and challenges for the Australian context. *Geoenergy Science and Engineering* 2023; 231:212354.
- Navaid HB, Emadi H, Watson M. A comprehensive literature review on the challenges associated with underground hydrogen storage. *Int J Hydrogen Energy* 2023;48:10603–35.
- Marchenko OV, Solomin SV. The future energy: hydrogen versus electricity. *Int J Hydrogen Energy* 2015;40:3801–5.
- Huang T, Moridis GJ, Blasingame TA, Abdulkader AM, Yan B. Compositional reservoir simulation of underground hydrogen storage in depleted gas reservoirs. *Int J Hydrogen Energy* 2023;48: 36035–50.
- Gahleitner G. Hydrogen from renewable electricity: an international review of power-to-gas pilot plants for stationary applications. *Int J Hydrogen Energy* 2013; 38:2039–61.
- Ozturk M, Dincer I. A comprehensive review on power-to-gas with hydrogen options for cleaner applications. *Int J Hydrogen Energy* 2021;46:31511–22.
- Ishaq H, Dincer I. Comparative assessment of renewable energy-based hydrogen production methods. *Renew Sustain Energy Rev* 2021;135:110192.
- Krevor S, De Coninck H, Gasda SE, Ghaleigh NS, de Gooyert V, Hajibeygi H, et al. Subsurface carbon dioxide and hydrogen storage for a sustainable energy future. *Nat Rev Earth Environ* 2023;4:102–18.
- Keshavarz A, Abid H, Ali M, Iglauer S. Hydrogen diffusion in coal: implications for hydrogen geo-storage. *J Colloid Interface Sci* 2022;608:1457–62.
- Wang S, Chen F, Wu Y-S, Nasrabadi H. The potential of hydrogen storage in depleted unconventional gas reservoirs: a multiscale modeling study. *Int J Hydrogen Energy* 2023;48:16007–19.
- Kutchko BG, Goodman AL, Rosenbaum E, Natesakhawat S, Wagner K. Characterization of coal before and after supercritical CO₂ exposure via feature relocation using field-emission scanning electron microscopy. *Fuel* 2013;107: 777–86.
- Arif M, Rasool Abid H, Keshavarz A, Jones F, Iglauer S. Hydrogen storage potential of coals as a function of pressure, temperature, and rank. *J Colloid Interface Sci* 2022;620:86–93.
- Liu A, Liu S. Hydrogen sorption and diffusion in coals: implications for hydrogen geo-storage. *Appl Energy* 2023;334:120746.
- Iglauer S, Abid H, Al-Yaseri A, Keshavarz A. Hydrogen adsorption on sub-bituminous coal: implications for hydrogen geo-storage. *Geophys Res Lett* 2021;48: e2021GL092976.
- Wang G, Chen W. Molecular simulations of hydrogen adsorption on coal with different ranks: implications for hydrogen geo-storage. *Int J Hydrogen Energy* 2024;51:10–20.
- Sambo C, Dudun A, Samuel SA, Esenenjor P, Muhammed NS, Haq B. A review on worldwide underground hydrogen storage operating and potential fields. *Int J Hydrogen Energy* 2022;47:22840–80.
- Godec ML, Jonsson H, Basava-Reddi L. Potential global implications of gas production from shales and coal for geological CO₂ storage. *Energy Proc* 2013;37: 6656–66.
- Iglauer S, Akhondzadeh H, Abid H, Paluszny A, Keshavarz A, Ali M, et al. Hydrogen flooding of a coal core: effect on coal swelling. *Geophys Res Lett* 2022;49: e2021GL096873.
- Liu J, Chen Z, Elsworth D, Miao X, Mao X. Evolution of coal permeability from stress-controlled to displacement-controlled swelling conditions. *Fuel* 2011;90: 2987–97.
- Rani S, Padmanabhan E, Prusty BK. Review of gas adsorption in shales for enhanced methane recovery and CO₂ storage. *J Petrol Sci Eng* 2019;175:634–43.
- Lu Y, Kang Y, Ramakrishna S, You L, Hu Y. Enhancement of multi-gas transport process in coalbed methane reservoir by oxidation treatment: based on the change of the interaction force between coal matrix and gas molecules and knudsen number. *Int J Hydrogen Energy* 2023;48:478–94.
- Shi JQ, Durucan S. Drawdown induced changes in permeability of coalbeds: a new interpretation of the reservoir response to primary recovery. *Transport Porous Media* 2004;56:1–16.
- Gao Q, Liu J, Zhao Y, Wei M, Leong Y-K, Elsworth D. A multiphysics model for biogenic gas extraction from coal seams. *Geoenergy Science and Engineering* 2023; 228:212045.
- Liu H-H, Rutqvist J. A new coal-permeability model: internal swelling stress and fracture–matrix interaction. *Transport Porous Media* 2009;82:157–71.
- Cui X, Bustin RM, Chikatamarla L. Adsorption-induced coal swelling and stress: implications for methane production and acid gas sequestration into coal seams. *J Geophys Res* 2007;112.
- Huang Y, Liu J, Elsworth D, Leong Y-K. A transient dual porosity/permeability model for coal multiphysics. *Geomechanics and Geophysics for Geo-Energy and Geo-Resources* 2022;8.
- Shi R, Liu J, Wei M, Elsworth D, Wang X. Mechanistic analysis of coal permeability evolution data under stress-controlled conditions. *Int J Rock Mech Min Sci* 2018; 110:36–47.
- Xiao Z, Wang G, Wang C, Jiang Y, Jiang F, Zheng C. Permeability evolution and gas flow in wet coal under non-equilibrium state: considering both water swelling and process-based gas swelling. *Int J Min Sci Technol* 2023;33:585–99.
- Mitra A, Harpalani S, Liu S. Laboratory measurement and modeling of coal permeability with continued methane production: Part 1–Laboratory results. *Fuel* 2012;94:110–6.
- Lv Z, Liu P, Zhao Y. Experimental study on the effect of gas adsorption on the effective stress of coal under triaxial stress. *Transport Porous Media* 2021;137: 365–79.
- Espinoza DN, Vandamme M, Pereira JM, Dangla P, Vidal-Gilbert S. Measurement and modeling of adsorptive-poromechanical properties of bituminous coal cores exposed to CO₂: adsorption, swelling strains, swelling stresses and impact on fracture permeability. *Int J Coal Geol* 2014;134–135:80–95.
- Zhang H, Liu J, Elsworth D. How sorption-induced matrix deformation affects gas flow in coal seams: a new FE model. *Int J Rock Mech Min Sci* 2008;45:1226–36.
- Palmer I, Mansoori J. How permeability depends on stress and pore pressure in coalbeds: a new model. *SPE Reservoir Eval Eng* 1998;1:539–44.
- Murakami Y. Theory of elasticity and stress concentration. John Wiley & Sons; 2016.
- Peng Y, Liu J, Wei M, Pan Z, Connell LD. Why coal permeability changes under free swellings: new insights. *Int J Coal Geol* 2014;133:35–46.
- Gensterblum Y, Ghanizadeh A, Cuss RJ, Amann-Hildenbrand A, Krooss BM, Clarkson CR, et al. Gas transport and storage capacity in shale gas reservoirs – a review. Part A: transport processes. *Journal of Unconventional Oil and Gas Resources* 2015;12:87–122.
- Vandamme M. Coupling between adsorption and mechanics (and vice versa). *Current Opinion in Chemical Engineering* 2019;24:12–8.
- Lv A, Ali Aghighi M, Masoumi H, Roshan H. On swelling stress–strain of coal and their interaction with external stress. *Fuel* 2022;311:122534.
- Terzaghi Kv. The shearing resistance of saturated soils and the angle between the planes of shear. *First international conference on soil Mechanics*, 1936/1936. p. 54–59.
- Sang G, Elsworth D, Liu S, Harpalani S. Characterization of swelling modulus and effective stress coefficient accommodating sorption-induced swelling in coal. *Energy Fuels* 2017;31:8843–51.
- Liu S, Harpalani S. Determination of the effective stress law for deformation in coalbed methane reservoirs. *Rock Mech Rock Eng* 2014;47:1809–20.
- Wang Z, Qin Y, Shen J, Li T, Zhang X, Cai Y. A novel permeability prediction model for coal based on dynamic transformation of pores in multiple scales. *Energy* 2022; 257:124710.

- [47] Pini R, Ottiger S, Burlini L, Storti G, Mazzotti M. Role of adsorption and swelling on the dynamics of gas injection in coal. *J Geophys Res Solid Earth* 2009;114.
- [48] Lin W, Kovscek AR. Gas sorption and the consequent volumetric and permeability change of coal I: experimental. *Transport Porous Media* 2014;105:371–89.
- [49] Lu M, Connell L. Coal failure during primary and enhanced coalbed methane production — theory and approximate analyses. *Int J Coal Geol* 2016;154–155: 275–85.
- [50] Zhao Y, Cui D, Liu J, Wei M, Liu Y. Evolution of coal permeability under constant effective stresses: direct measurements and numerical modeling. *Energy Fuels* 2021;35:15489–501.
- [51] Lu M, Connell LD. Swell of coal matrix induced by gas sorption and its partition to pore volume and bulk strains—a critical parameter for coal permeability. In: 44th US rock mechanics symposium and 5th US-Canada rock mechanics symposium. OnePetro; 2010.
- [52] Nie X, Chen J, Cao Y, Gong D, Deng H. Analysis of coal swelling deformation caused by carbon dioxide adsorption based on X-Ray computed tomography. *Geofluids* 2018;2018:6939827.
- [53] Manovic V, Loncarevic D, Tokalic R. Particle-to-Particle heterogeneous nature of coals—a case of large coal particles. *Energy Sources, Part A Recovery, Util Environ Eff* 2009;31:427–37.
- [54] Sander R, Pan Z, Connell LD. Laboratory measurement of low permeability unconventional gas reservoir rocks: a review of experimental methods. *J Nat Gas Sci Eng* 2017;37:248–79.
- [55] Qin X, Cai J, Wang G. Pore-scale modeling of pore structure properties and wettability effect on permeability of low-rank coal. *Int J Min Sci Technol* 2023;33: 573–84.
- [56] Karacan C. Swelling-induced volumetric strains internal to a stressed coal associated with CO₂ sorption. *Int J Coal Geol* 2007;72:209–20.
- [57] Sampath KHSM, Perera MSA, Li D-y, Ranjith PG, Matthai SK. Evaluation of the mechanical behaviour of brine+CO₂ saturated brown coal under mono-cyclic uni-axial compression. *Eng Geol* 2019;263:105312.
- [58] Zhang Y, Lebedev M, Sarmadivaleh M, Barifcani A, Iglauer S. Swelling-induced changes in coal microstructure due to supercritical CO₂ injection. *Geophys Res Lett* 2016;43:9077–83.
- [59] Lv A, Bahaaddini M, Masoumi H, Roshan H. The combined effect of fractures and mineral content on coal hydromechanical response. *Bull Eng Geol Environ* 2022; 81:1–20.
- [60] Kang J, Elsworth D, Fu X, Liang S, Chen H. Contribution of thermal expansion on gas adsorption to coal sorption-induced swelling. *Chem Eng J* 2022:432.
- [61] Liu S, Wang Y, Harpalani S. Anisotropy characteristics of coal shrinkage/swelling and its impact on coal permeability evolution with CO₂ injection. *Greenhouse Gases: Sci Technol* 2016;6:615–32.
- [62] Connell LD, Lu M, Pan Z. An analytical coal permeability model for tri-axial strain and stress conditions. *Int J Coal Geol* 2010;84:103–14.
- [63] Tang S, Wan Y, Duan L, Xia Z, Zhang S. Methane adsorption-induced coal swelling measured with an optical method. *Int J Min Sci Technol* 2015;25:949–53.
- [64] Li Y, Tang D, Xu H, Meng Y, Li J. Experimental research on coal permeability: the roles of effective stress and gas slippage. *J Nat Gas Sci Eng* 2014;21:481–8.
- [65] Chen Z, Pan Z, Liu J, Connell LD, Elsworth D. Effect of the effective stress coefficient and sorption-induced strain on the evolution of coal permeability: experimental observations. *Int J Greenh Gas Control* 2011;5:1284–93.
- [66] Cui X, Bustin RM. Volumetric strain associated with methane desorption and its impact on coalbed gas production from deep coal seams. *AAPG (Am Assoc Pet Geol) Bull* 2005;89:1181–202.
- [67] Mazumder S, Karnik A, Wolf KH. Swelling of coal in response to CO₂ sequestration for ECBM and its effect on fracture permeability. *SPE J* 2006;11:390–8.
- [68] Robertson EP. Modeling permeability in coal using sorption-induced strain data. In: SPE annual technical conference and exhibition; 2005. SPE-97068-MS.
- [69] Zhao Y, Zhao Y, Liu J, Wei M, Cui D, Gao S. Coal permeability behaviors and non-uniform deformations under various boundary conditions: Part 1 – experimental observations. *Fuel* 2023;341:127649.
- [70] Shi J-Q, Durucan S. A model for changes in coalbed permeability during primary and enhanced methane recovery. *SPE Reservoir Eval Eng* 2005;8:291–9.
- [71] Jiang C, Zhao Z, Zhang X, Liu J, Elsworth D, Cui G. Controlling effects of differential swelling index on evolution of coal permeability. *J Rock Mech Geotech Eng* 2020;12:461–72.
- [72] Zhao Y, Zhao Y, Liu J, Wei M, Huang Y, Jiang C. Coal permeability behaviors and non-uniform deformations under various boundary conditions: Part 2 – modelling study. *Fuel* 2023;343:127914.
- [73] Liu S, Harpalani S, Pillalamarry M. Laboratory measurement and modeling of coal permeability with continued methane production: Part 2—Modeling results. *Fuel* 2012;94:117–24.
- [74] Liu S, Harpalani S. Evaluation of in situ stress changes with gas depletion of coalbed methane reservoirs. *J Geophys Res Solid Earth* 2014;119:6263–76.
- [75] Zhang X, Jin C, Zhang D, Zhang C, Ranjith PG, Yuan Y. Carbon dioxide flow behaviour in macro-scale bituminous coal: an experimental determination of the influence of effective stress. *Energy* 2023;268:126754.
- [76] Zhang X, Wu C, Wang Z. Experimental study of the effective stress coefficient for coal permeability with different water saturations. *J Petrol Sci Eng* 2019;182: 106282.
- [77] Gercek H. Poisson's ratio values for rocks. *Int J Rock Mech Min Sci* 2007;44:1–13.
- [78] Al-Bazali T, Zhang J, Chenevert ME, Sharma MM. Factors controlling the compressive strength and acoustic properties of shales when interacting with water-based fluids. *Int J Rock Mech Min Sci* 2008;45:729–38.
- [79] Perera MSA, Sampath KHSM. Modelling of free and adsorbed CO₂-induced mechanical property alterations in coal. *Int J Coal Geol* 2020;217:103348.
- [80] Lu S, Li L, Cheng Y, Sa Z, Zhang Y, Yang N. Mechanical failure mechanisms and forms of normal and deformed coal combination containing gas: model development and analysis. *Eng Fail Anal* 2017;80:241–52.